# Quaternion Based Omnidirectional Machine Condition Monitoring System

**Wai-Kit Wong**                                                        *wkwong@mmu.edu.my*
*Faculty of Engineering and Technology,*
*Multimedia University,*
*75450 JLN Ayer Keroh Lama,*
*Melaka, Malaysia.*


**Chu-Kiong Loo**                                                        *ckloommu@gmail.com*
*Faculty of Computer Science and Information Technology*
*University of Malaya*
*50603 Lembah Pantai*
*Kuala Lumpur, Malaysia.*


**Way-Soong Lim**                                                        *wslim@mmu.edu.my*
*Faculty of Engineering and Technology,*
*Multimedia University,*
*75450 JLN Ayer Keroh Lama,*
*Melaka, Malaysia.*

## Abstract

Thermal monitoring is useful for revealing some serious electrical problems in a factory that often go undetected until a serious breakdown occurs. In factories, there are various types of functioning machines to be monitored. When there is any malfunctioning of a machine, extra heat will be generated which can be picked up by thermal camera for image processing and identification purpose. In this paper, a new and effective omnidirectional machine condition monitoring system applying log-polar mapper, quaternion based thermal image correlator and max-product fuzzy neural network classifier is proposed for monitoring machine condition in an omnidirectional view. With this monitoring system, it is convenient to detect and monitor the conditions of (overheat or not) of more than one machines in an omnidirectional view captured by using a single thermal camera. Log-polar mapping technique is used to unwarp omnidirectional thermal image into panoramic form. Two classification characteristics namely: peak to sidelobe ratio (PSR) and real to complex ratio of the discrete quaternion correlation output (p-value) are applied in the proposed machine condition monitoring system. Large PSR and p-value observe in a good match among correlation of the input thermal image with a particular reference image, while small PSR and p-value observe in a bad/not match among correlation of the input thermal image with a particular reference image. Simulation results also show that the proposed system is an efficient omnidirectional machine monitoring system with accuracy more than 97%

**Keywords:** Machine Condition Monitoring System, Neuro Fuzzy System, Thermal Imaging, Quaternion, Omnidirectional.

## 1. INTRODUCTION

Many factories in all over the world rely on machines to help improve their production and process. An effective machine condition monitoring system play an important role in those factories to ensure that their production and process are running smoothly all the time. Infrared cameras or thermal cameras are used in many heavy factories for monitoring the temperature conditions of the machines. When there is any malfunctioning of machines, extra heat will be generated and it can be picked up by thermal camera. Thermal camera will generate an image to indicate the condition of the machine. This enables the operator to decide on the on/off switch. Any malfunctioned machines detected will proceed to further repairmen action. This process is term as thermal imaging monitoring.

Wai-Kit Wong, Chu-Kiong Loo & Way-Soong Lim

Thermal imaging monitoring is more convenient in compare to conventional maintenance method. In conventional maintenance method, functioning machines needs to be frequently monitored by operator. The problem is it required more man power and longer maintenance time. However, with thermal imaging monitoring, the operating machines can be maintained and monitored by the operator with observing the thermal images captured routinely on the functioning machines and display on a monitor, even from a remote location. So, hands on workload, man power, maintenance time can be reduced and improve safety, since some overheat devices cannot see through eyes, but can read from thermal images, hence the use of thermal imaging monitoring can prevent accident happen too [1].

If a single thermal camera is applied to monitor a single machine, then for more functioning machines in different angle of view, more thermal cameras are required. This will increase cost, beside complicated the monitoring network. In this paper, a new and effective omnidirectional machine condition monitoring system applying log-polar mapper, quaternion based thermal image correlator and max-product fuzzy neural network classifier is proposed for monitoring machine condition in an omnidirectional view. In terms of hardware part, an omnidirectional thermal imaging system consists of thermal camera, custom made IR reflected hyperbolic mirror, camera mirror holder, and laptop/PC as image processing tools is proposed for effective machine condition monitoring purpose. Thermal images captured from the custom made hyperbolic mirror are in omnidirectional view. Log-polar mapping technique [2] is applied for unwarping the captured omnidirectional thermal images into panoramic form, providing the observer or image processing tools a complete wide angle of view.

Quaternion correlator is so far commonly used in color human face recognition [3] and color alphanumeric words recognition [4]. It is found to be useful in machine condition monitoring too, especially in thermal condition monitoring. In [5], quaternion correlator was proposed to be used in thermal image recognition for machine condition monitoring system, so called the quaternion based thermal image correlator. The quaternion based thermal image correlator was in pair with max-product fuzzy neural network classifier were used to monitor fixed angle machines' condition. The experimental results in [5] also shown that the proposed system achieves high accuracy in monitoring machines condition. It's never been used in omnidirectional approach. Therefore, in this paper, quaternion based thermal image correlator and max-product fuzzy neural network classifier are proposed for omnidirectional machine condition monitoring system as a new approach.

In quaternion based thermal image correlator proposed in [5], a strong and sharp peak can be observed in the output correlation plane when the input thermal image comes from the authentic class (input thermal image matches with a particular training/reference image stored in the database), and there will be no discernible peak if the input thermal image comes from imposter class (input thermal image does not match with the particular reference image). For better recognition, peak-to-sidelobe ratio (PSR) [6] is introduced to test whether an input thermal image belongs to the authentic class or not. In [5], it is discovered that by considering the peak value with the region around the peak value is more accurate compare to just a single peak point. According to the results in [5], the higher is the value of PSR, the more likely is the input thermal image belonging to the reference image class. Another parameter use in [5] for quaternion correlation is the real to complex ratio of the discrete quaternion correlation output ($p$-value [4]). $p$-value is used in quaternion based thermal image correlator for measuring the quaternion correlation output between the colors, shape, size and brightness of the input thermal image and a particular reference thermal image.

A max-product fuzzy neural network classifier is also proposed to perform classification on the thermal images based on the PSR and $p$-value output from the quaternion based thermal image correlator. Classification in pattern recognition [7] refers to a procedure whereby individual patterns are placed into groups based on quantitative information on one or more characteristics inherent in the patterns and based on a training set of previously labeled patterns, known as classes. The purpose of classification is to establish a rule whereby a new observed pattern will map into one of the existing classes. These classes are predefined by a partition of the sample

space, which is the attributes themselves. For example, a machine may be classified as overheated if the colors display in the thermal image is brighter than the predetermined limits.

In [5], the max-product fuzzy neural network classifier was modified according to [8] to perform the classification in machine condition monitoring system. According to the designed max-product fuzzy neural network classifier, both the PSR and $p$-value output from the quaternion based thermal image correlator are first fuzzified with Gaussian membership function. The max-product fuzzy neural network classifier is applied for accurate classification with the weights obtained from training reference images. The weights are then applied for classification of input images in real time application. The same classifier is applied in this paper, for the omnidirectional approach. Experimental results show that in the authentic case, if an input image is well matched with a particular reference image in the database, followed by performing quaternion correlation on these two images, their output correlation plane will have sharp peaks. However in imposter case, if an input thermal image is not matched with a particular reference image in the database, the output correlation plane is flat. Large peak to sidelobe ratio (PSR) and real to complex ratio of the discrete quaternion correlation output ($p$-value) is proven to have a good match among correlation of the input thermal image with a particular reference image, while small PSR and $p$-value reflect reversely. Experimental results in this paper also show that the proposed system is an efficient wide angle coverage machine condition monitoring system with accuracy above 97%.

This paper is organized in the following order: Section 2 briefly comments on the quaternion based omnidirectional machine condition monitoring system, section 3 summarize the log-polar image geometry and the mapping techniques. The algorithm of the proposed quaternion based thermal image correlator is described in section 4. Section 5 describes the structure of the max-product fuzzy neural network classifier. In section 6, the experimental results is discussed. Finally section 7 summarizes the work and some suggestions are proposed for future work.

## 2. QUATERNION BASED OMNIDIRECTIONAL MACHINE CONDITION MONITORING SYSTEM MODEL

The quaternion based omnidirectional machine condition monitoring system developed in this paper is shown in Fig. 1.
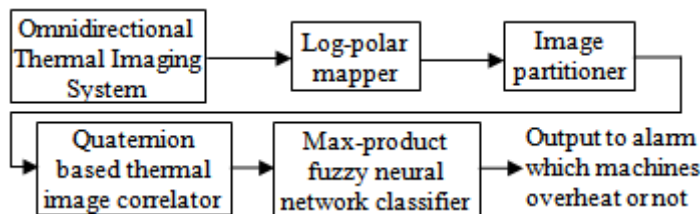


**FIGURE 1:** Quaternion based omnidirectional machine condition monitoring system

The omnidirectional thermal imaging system consists of three elements, which are the custom made IR reflected hyperbolic mirror, camera mirror holder set and thermal camera. The research group of OMNIVIEWS project from Czech Technical University developed MATLAB software for designing omnidirectional mirror [9]. Utilizing the MATLAB software, omnidirectional hyperbolic mirror can be designed by inputting some parameters specify the mirror dimension. The details of the mirror design can be found in [13]. The coordinates generated using MATLAB software as well as mechanical drawing using Autocad was provided to precision engineering company to fabricate/custom made the hyperbolic mirror. The hyperbolic mirror is milling by using aluminum bar and chrome plating with chromium. Chromium is selected because of its lustrous (good in IR reflection), high corrosion resistance, high melting point and hardness. The camera mirror holder is designed and custom made with aluminum material as shown in Fig. 2.

The thermal camera used in the proposed omnidirectional thermal imaging system is an affordable and accurate temperature measurement model: ThermoVision A-20M manufactured by FLIR SYSTEM [10]. The thermal camera has a temperature sensitivity of 0.10 in a range from

-20ºC to 900ºC and it can capture thermal image with fine resolution up to 320 X 240 pixels offering more than 76,000 individual measurement points per image at a refresh rate of 50/60 Hz. For fast image and data transfer of real-time fully radiometric 16-bit images, an IEEE-1394 FireWire digital output can be selected. For network and/or multiple camera installations, Ethernet connectivity is also available. Each A-20M can be equipped with its own unique URL allowing it to be addressed independently via its Ethernet connection and it can be linked together with router to form a network. Therefore, it is best outfitted for machine condition monitoring system in a big factory site.

Log-polar mapper applying log polar mapping techniques [2]. It unwarps the captured omnidirectional thermal image into panoramic form, provided observer or image processing tools



**FIGURE 2:** Overall fabricated omnidirectional thermal imaging system model.

a wide angle of view. Another merit of log-polar image representation is that it has data compression manner. Log-polar mapping has been used in [13] for unwarping omnidirectional thermal image for machine condition monitoring. Detailed discussion on log-polar mapping will be provided in Section 3. Image partitioner is used for partitioned the input thermal image into S-partitioned sections, provided that the input thermal image consisted of S machines to be monitored. Each partitioned section consists of one machine to be monitored. An example of a panoramic thermal image with S=3 partition sections is shown in Fig. 3.
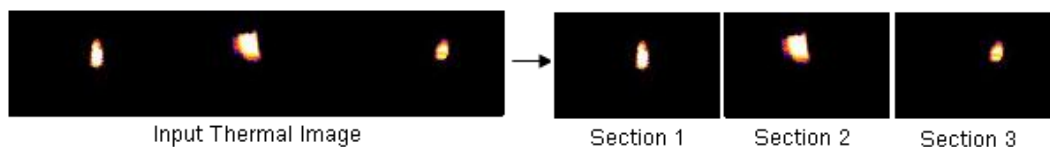


**FIGURE 3:** Example of a panoramic thermal image with S=3 partition sections.

Quaternion based thermal image correlator [5] is used to obtain correlation plane for each correlated input thermal image captured lively with reference images of all possible machines conditions stored in a database to calculate out some classification characteristics such as the real to complex ratio of the discrete quaternion correlation (DQCR) output, $p$-value and the peak-to-sidelobe ratio, PSR. These classification characteristics will later input to the max-product fuzzy neural network classifier to perform classification. Detailed discussion on quaternion based thermal image correlation will be performed in Section 4.

The max-product fuzzy neural network classifier [5] is first applied to train for an accurate classification with the weight ($w$) obtained form training reference images of all possible machines conditions stored in the database. During application, the PSR and $p$-value output from quaternion based thermal image correlator are first fuzzified into Gaussian membership function. Next, product value is calculated based on the multiplication of PSR in Gaussian membership value with $p$-value in Gaussian membership value. The product values are stored in an array and multiply with the weight ($w$). Max-composition is performing on the output based on two sets of fuzzy IF-THEN rules, and defuzzification is performed to classify each machine's condition under monitoring. Detailed discussion on max-product fuzzy neural network classifier will be given in Section 5.

## 3. LOG-POLAR MAPPING

Log-polar geometry or log-polar transform in short, is an example of foveated or space-variant image representation used in the active vision systems motivated by human visual system [11]. It is a spatially-variant image representation in which pixel separation increases linearly with distance from a central point [12]. It provides a way of concentrating computational resources on regions of interest, whilst retaining low-resolution information from a wider field of view. One merit of this kind of image mapping technique is data reduction. Foveal image representations like this are most useful in the context of active vision system where the densely sampled central region can be directed to pick up the most salient information. Mammalians especially human eyes are very roughly organized in this way.

In the software conversion of log-polar images, practitioners in pattern recognition usually named it as log-polar mapping [13]. According to [13], it is found out that the use of log-polar mapping having numbers of merits such as help solving rotation and scaling problems in quaternion based thermal image correlation. However, the main merit of log-polar mapping to be applied in this paper is that it can unwarp/convert an omnidirectional image into panoramic image, hence providing the observer and image processing tools a complete wide angle of view for the surveillance area's surroundings and preserving fine output image quality in a higher data compression manner.
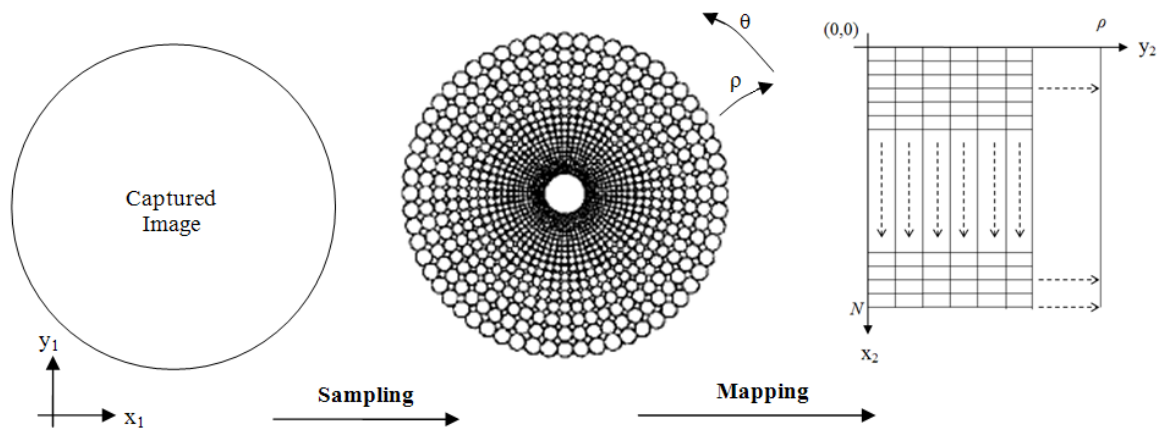


**FIGURE 4 :** A graphical view of log-polar mapping.

The spatially-variant grid that represents log-polar mapping is formed by $i$ number of concentric circles with $N$ samples over each concentric circle [11]. An example of a spatially-variant sampling grid is shown in Fig. 4.

The log-polar mapping use in this paper can be summarized as following [13]: Initially, omnidirectional thermal image is captured using the omnidirectional thermal imaging system as shown in Fig. 2. The geometry of the captured omnidirectional thermal image is in Cartesian form $(x_1,y_1)$. Next, the Cartesian omnidirectional thermal image is sampled by the spatially-variant grid into a log-polar form $(\rho,\theta)$ omnidirectional thermal image. After that, the log-polar omnidirectional

thermal image is unwarped into a panoramic thermal image $(x_2, y_2)$, another Cartesian form. Since the panoramic thermal image is in Cartesian form, subsequent image processing task will become much easier.

The centre of pixel for log-polar sampling is described by [2]:

$$\rho(x_1, y_1) = \log_\lambda \frac{R}{r_o} \tag{1}$$

$$\theta(x_1, y_1) = \frac{N_\theta}{2\pi} \arctan \frac{y_1}{x_1} \tag{2}$$

The centre of pixel for log-polar mapping is described by [2]:

$$x_2(\rho, \theta) = \lambda^\rho r_o \cos\left(\frac{2\pi\theta}{N_\theta}\right) \tag{3}$$

$$y_2(\rho, \theta) = \lambda^\rho r_o \sin\left(\frac{2\pi\theta}{N_\theta}\right) \tag{4}$$

where $R$ is the distance between the given point and the center of mapping $= \sqrt{x_1^2 + y_1^2}$

$r_o$ is a scaling factor which will define the size of the circle at $\rho(x_1, y_1) = 0$.

$\lambda$ is the base of the algorithm,

$$\lambda = \frac{1 + \sin \dfrac{\pi}{N_\theta}}{1 - \sin \dfrac{\pi}{N_\theta}} \tag{5}$$

$N_\theta$ is the total number of pixels per ring in log-polar geometry. This value is assigned by user. For eg: if user assign $N_\theta$=5, the ring is divided into 5 sectors or 5 pixels per ring. If $N_\theta$=100, each ring is divided into 100 sectors or 100 pixels per ring. The higher the $N_\theta$, the higher the resolution in $\theta$-axis (angular). Refer [2] for detailed discussion on this issue.

The number of rings in the fovea region is given by [2]:
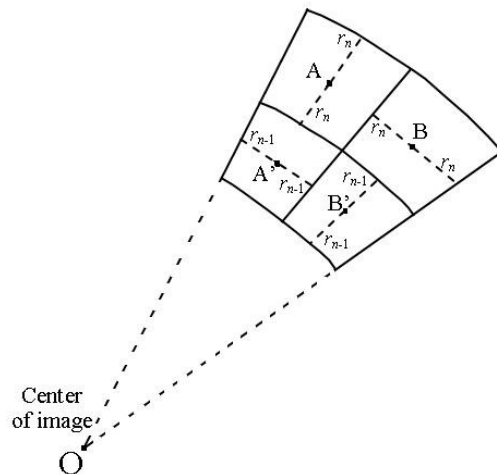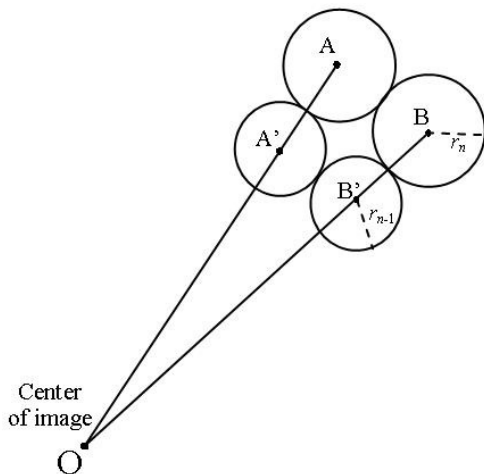
$$N_{fov} = \frac{\lambda}{\lambda - 1} \tag{6}$$



**FIGURE 5 :** Conventional circular sampling method for Log-Polar image.  **FIGURE 6 :** Sector sampling method for log polar image.
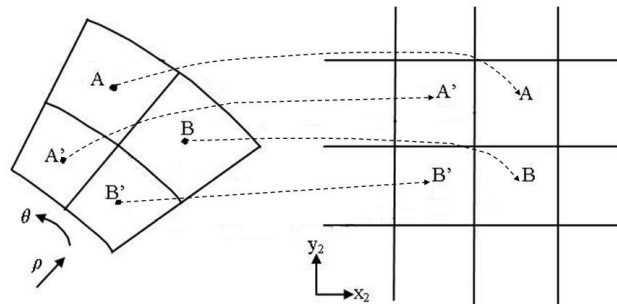
**FIGURE 7 :** Unwarping process

The number of rings must be an integer. Hence, the calculated $N_{fov}$ is rounded to the closer integer value. To sample the Cartesian pixels (x₁, y₁) into log polar pixels ($\rho$, $\theta$), at each center point calculated using (1) and (2), the corresponding log-polar pixel ($\rho_n$, $\theta_n$) is cover a region of Cartesian pixels with radius:

$$r_n = \lambda r_{n-1} \qquad (7)$$

where *n*=0, 1, …, N-1. Fig. 5 shows the conventional circle sampling method of log-polar mapping [11, 14].

One of the demerits of using circle sampling is that certain region of Cartesian pixels outsides sampling circle did not cover by any log-polar pixels. Therefore, some researchers [5, 15-17] had come out with sector sampling method as shown in Fig. 6, which could maximize the coverage of Cartesian pixels for each log polar pixel. The region of Cartesian pixels covers by an individual log-polar pixel will has the same color intensity follow the respective original Cartesian center sampling point.

During unwarping process, the ($\rho$, $\theta$) pixels will map to each corresponding (x₂, y₂) pixels as shown in Fig. 7. The region of Cartesian pixels on the panoramic image (x₂,y₂) is covered by an individual log-polar pixel on the log-polar ($\rho$,$\theta$) omnidirectional image. Therefore, the pixels in that specific region on the panoramic image (x₂,y₂) will have the same intensity with respect to the corresponding individual log-polar pixel.

## 4. QUATERNION BASED THERMAL IMAGE CORRELATOR
In this section, the algorithm of the quaternion based image correlator as proposed in [5] will be discussed.

### 4.1 Algorithm For Quaternion Based Thermal Image Correlator
The reference image after performing discrete quaternion Fourier transforms (DQFT) [4] is given by:

$$I(\mathrm{m,n}) = I_R(\mathrm{m,n}).i + I_G(\mathrm{m,n}).j + I_B(\mathrm{m,n}).k \qquad (8)$$

where m, n are the pixel coordinates of the reference image. R, G, B parts of reference image are represented by $I_R(\mathrm{m,n})$, $I_G(\mathrm{m,n})$ and $I_B(\mathrm{m,n})$ respectively, and *i-, j-, k-* are the imaginary parts of quaternion complex number [18], whereby the real part of it is set to zero. Similarly, $h_i(\mathrm{m,n})$ is used for representing input image. Then, output $b(\mathrm{m,n})$ can be produced to conclude whether the input image matches the reference image or not. If $h_i(\mathrm{m,n})$ is the space shift of the reference image:

$$h_i(\mathrm{m,n}) = I(\mathrm{m-m_0, n-n_0}) \qquad (9)$$

then after some calculation,

$$\text{Max}(b_r(m,n)) = b_r(-m_0, n_0) \qquad (10)$$

where $b_r(m,n)$ means the real part of $b(m,n)$ and

$$b_r(-m_0, n_0) = \sum_{m=0}^{M-1}\sum_{n=0}^{N-1}|I(m,n)|^2 \qquad (11)$$

where M, N is the image x-axis, y-axis dimension. At the location $(-m_0, n_0)$, the multiplier of $i$-, $j$-, $k$-imaginary part of $b(-m_0, n_0)$ are equal to zero:

$$b_i(-m_0, n_0) = b_j(-m_0, n_0) = b_k(-m_0, n_0) = 0 \qquad (12)$$

Hence, the process as below for thermal image correlation is followed [5]:

1.) Calculate energy of reference image $I(m,n)$ :

$$E_I = \sum_{m=0}^{M-1}\sum_{n=0}^{N-1}|I(m,n)|^2 \qquad (13)$$

Then the reference image $I(m,n)$ and the input image $h_i(m,n)$ are normalized as:

$$I_a(m,n) = I(m,n)\big/\sqrt{E_I} \qquad (14)$$

$$H_a(m,n) = h_i(m,n)\big/\sqrt{E_I} \qquad (15)$$

2.) Calculate the output of discrete quaternion correlation (DQCR):

$$g_a(m,n) = \sum_{\tau=0}^{M-1}\sum_{\eta=0}^{N-1}I_a(\tau,\eta).\overline{H_a(\tau-m, \eta-n)} \qquad (16)$$

where ' $\overline{\phantom{xx}}$ ' means the quaternion conjugation operation and perform the space reverse operation:

$$g(m,n) = g_a(-m, -n) \qquad (17)$$

3.) Perform inverse discrete quaternion Fourier Transform (IDQFT) on (17) to obtain the correlation plane $P(m,n)$.

4.) Search all the local peaks on the correlation plane and record the location of the local peaks as $(m_s, n_s)$.

5.) Then at all the location of local peaks $(m_s, n_s)$ found in step 4, we calculate the real to complex value of the DQCR output is calculated:

$$p = \frac{|P_r(m_s, n_s)|}{|P_r(m_s, n_s)| + |P_i(m_s, n_s)| + |P_j(m_s, n_s)| + |P_k(m_s, n_s)|} \qquad (18)$$

where $P_r(m_s, n_s)$ is the real part of $P(m_s, n_s)$. $P_i(m_s, n_s)$, $P_j(m_s, n_s)$ and $P_k(m_s, n_s)$ are the $i$-, $j$-$k$- parts of $P(m_s, n_s)$ respectively. If $p \ge d_1$ and $c_1 < |P(m_s, n_s)| < c_2$, then it can be concluded that at location $(m_s, n_s)$, there is an object that has the same shape, size, color and brightness as the reference image. $d_1 < 1$, $c_1 < 1 < c_2$ and $c_1$, $c_2$ and $d_1$ are all with values near to 1. The

value of p decays faster with the color difference among the match image to the reference image.

Another classification characteristic proposed in quaternion based thermal image correlation by [5] is the peak-to-sidelobe ratio (PSR) which will be discussed in details as below. The quaternion based thermal image correlation involved 2 stages [5]: 1. Enrollment stage, and 2. Recognition stage. During the enrollment stage, one or multiple panoramic thermal images of each machine condition are acquired. These multiple reference images should have the variability in the color tones for different temperature conditions of the machines. The DQFT of the reference images are used to train fuzzy neural network and determine correlation filter for each possible machines' conditions. During recognition stage, omnidirectional thermal imaging system captures a live omnidirectional machines' thermal image, unwarps it into panoramic thermal image, and the DQFT of such image is correlated with the DQFT form of the reference images stored in the
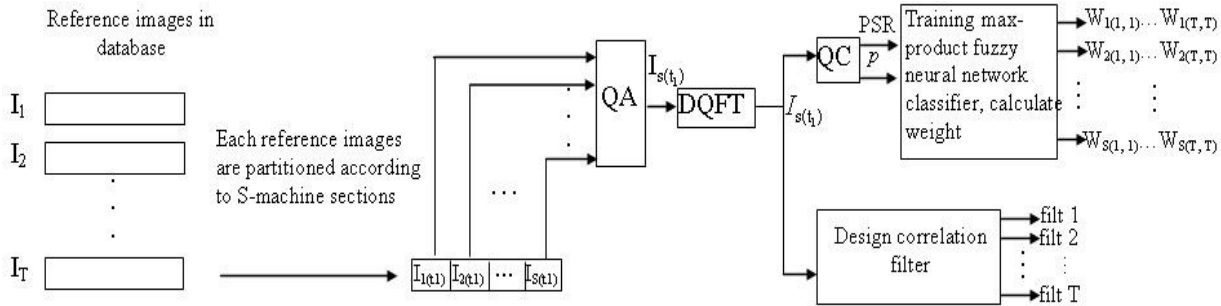


**FIGURE 8 :** Schematic of enrollment stage

database together with their corresponding filter coefficients, and the inverse DQFT of this product results in the correlation output for that filter.

A strong peak can be observed in the correlation output if the input image comes from imposter class. A method of measuring the peak sharpness is the peak-to-sidelobe ratio (PSR) which is defined as below [3, 5]:

$$\text{PSR} = \frac{peak - mean(sidelobe)}{\sigma(sidelobe)} \qquad (19)$$

where *peak* is the value of the peak on the correlation output plane. *sidelobe* refers a fixed-sized surrounding area off the peak. *mean* is the average value of the sidelobe region. $\sigma$ is the standard deviation of the sidelobe region. Large PSR values indicate the better match of the input image and the corresponding reference image. Enrollment stage and recognition stage are discussed in details in next subsections.

**4.2 Enrollment Stage**
The schematic of enrollment stage for quaternion based thermal image correlator as proposed in [5] is shown in Fig. 8. To be applied in omnidirectional approach in this paper, during the enrollment stage, the reference panoramic thermal images for each possible machine's conditions in database are partitioned according to S machine sections. Each machine section consists of one single machine to be monitored. S is the total number of machines to be monitored. These partitioned reference images are then encoded into a two dimensional quaternion array (QA) as follows [5]:

$$I_{s(t_1)} = I_{sr(t_1)} + I_{sR(t_1)}.i + I_{sG(t_1)}.j + I_{sB(t_1)}.k \qquad (20)$$

where $t_1 = 1, 2, \ldots, T$ represents the number of reference images, $I_{sr(t_1)}$ represents the real part of quaternion array of s-th machine section for reference image $t_1$, s = 1, 2, …, S represents the

number of partitioned machines' sections. $I_{sR(t_1)}$, $I_{sG(t_1)}$ and $I_{sB(t_1)}$ each represents the $i$-, $j$-, $k$-imaginary part of s-th machine section for reference image $t_1$ respectively.

The quaternion array in (20) is then performs discrete quaternion Fourier transform (DQFT) to transform the quaternion image to the quaternion frequency domain. A two-side form of DQFT has been proposed by Ell [19, 20] as follows:

$$I_{s(t_1)}(m, n) = \sum_{\tau=0}^{M-1}\sum_{\eta=0}^{N-1} e^{-\mu_1 2\pi(m\tau/M)}.I_{s(t_1)}(\tau, \eta).e^{-\mu_2 2\pi(n\eta/N)}$$

(21)

where $e$ is exponential term, $\mu_1$ and $\mu_2$ are two units pure quaternion (the quaternion unit with real part equal to zero) that are orthogonal to each other [21]:

$$\mu_1 = \mu_{1,i}.i + \mu_{1,j}.j + \mu_{1,k}.k \qquad (22)$$

$$\mu_2 = \mu_{2,i}.i + \mu_{2,j}.j + \mu_{2,k}.k \qquad (23)$$

$$\mu_{1,i}^2 + \mu_{1,j}^2 + \mu_{1,k}^2 = \mu_{2,i}^2 + \mu_{2,j}^2 + \mu_{2,k}^2 = 1$$

$$(\text{i.e}: \ \mu_1^2 = \mu_2^2 = -1) \qquad (24)$$

$$\mu_{1,i}.\mu_{2,i} + \mu_{1,j}.\mu_{2,j} + \mu_{1,k}.\mu_{2,k} = 0 \qquad (25)$$

The output of DQFT, $I_{s(t_1)}$ is used to train the max-product fuzzy neural network classifier and design the correlation filter.

### 4.2.1 Quaternion Correlator (QC)
To train the max-product fuzzy neural network classifier, the output of the DQFT is first passed to a quaternion correlator (QC) as shown in Fig. 9 [5].
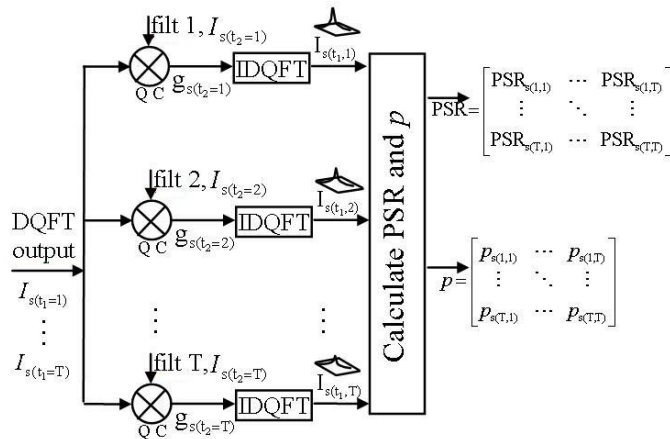


**FIGURE 8 :** Quaternion correlator (QC)

The function of the QC is summarized as below [5]: For DQFT output of s-th machine section, perform discrete quaternion correlation (DQCR) [22, 23] on reference image $I_{s(t_1)}$ with reference image $I_{s(t_2)}$ and multiply with corresponding filter coefficients (filt$_{(t2)}$):

$$g_{s(t_1, t_2)}(m, n) = \sum_{\tau=0}^{M-1}\sum_{\eta=0}^{N-1} I_{s(t_1)}.\overline{I_{s(t_2)}(\tau - m, \eta - n)}. \text{filt}_{(t_2)} \qquad (26)$$

where $t_1, t_2 = 1, 2, \ldots, T$ are the number of reference image. After that, (26) is performing inverse DQFT to obtain the correlation plane function:

$$P_{s(t_1,t_2)}(m,n) = \frac{1}{4\pi^2} \sum_{\tau=0}^{M-1}\sum_{\eta=0}^{N-1} e^{-\mu_1 2\pi(m\tau/M)} \cdot g_{s(t_1,t_2)}(m,n) \cdot e^{-\mu_2 2\pi(n\eta/N)} \qquad (27)$$

The correlation plane is a collection of correlation values, each one obtained by performing a pixel-by pixel comparison (inner product) of two images ($I_{s(t_1)}$ and $I_{s(t_2)}$). A sharp peak in the correlation plane indicate the similarity of $I_{s(t_1)}$ and $I_{s(t_2)}$, while the absence or lower of such peak indicate the dissimilarity of $I_{s(t_1)}$ and $I_{s(t_2)}$.

Calculate $p_{s(t_1,t_2)}$ and $\mathrm{PSR}_{s(t_1,t_2)}$ from the correlation plane as in (27) using (18) and (19) respectively. $p_{s(t_1,t_2)}$ means $p$-values of reference image $I_{(t_1)}$ correlate on reference image $I_{(t_2)}$ in s-th machine section, while $\mathrm{PSR}_{s(t_1,t_2)}$ means PSR values of reference image $I_{(t_1)}$ correlate on reference image $I_{(t_2)}$ in s-th machine section. These values are then feed into max-product fuzzy neural network classifier to perform training and calculate weight, which will be presented in section 5.

**4.2.2 Correlation Filter Selection**
According to research justification work done in [5], correlation filter outperforms conventional matched filters in filtering nonlinear image distortion (scale, rotation and pose invariant). Among the correlation filter, the minimum average correlation energy (MACE) filters [26] show good results in the field of automatic target recognition, face recognition and applications in biometric verification [6, 27]. MACE filters are using more than one reference image to synthesize a single filter template, therefore making its classification performance invariant to shift of the input image [25].

There are three types of MACE filters in general, namely: 1.) Conventional MACE filter [26], 2.) Unconstrained MACE (UMACE) filter [28] and 3.) Unconstrained optimal tradeoff synthetic discriminant filter (UOTSDF), all with the goal to produce sharp peaks that resemble two dimensional delta-type correlation outputs when the input image belongs to the authentic class and low peaks in imposter class. Conventional MACE filter [26] minimizes the average correlation energy of the reference images while constraining the correlation output at the origin to a specific value (usually 1), for each of the reference images. Lagrange multiplier is used for optimization, yielding:

$$\mathrm{filt}_{\mathrm{MACE}} = D^{-1}X(X'D^{-1}X)^{-1}c \qquad (28)$$

This equation is the closed form solution to be the linear constrained quadratic minimization. D is diagonal matrix with the average power spectrum of the reference images placed as elements along diagonal of the matrix. X contains Fourier transform of the reference images lexicographically re-ordered and placed along each column. As an example, if there are T thermal reference images of size $282\times 60 (=16920)$, then X will be a $16920\times T$ matrix. X' is the matrix transpose of X. c is a column vector of length T with all entries equal to 1.

The second type of MACE filter is the unconstrained MACE (UMACE) filter [28]. Just like conventional MACE filter, UMACE filter also minimizes the average correlation energy of the reference images and maximizes the correlation output at the origin. The different between conventional MACE filter and UMACE filter is the optimization scheme. Conventional MACE filter is using Lagrange multiplier but as for UMACE filter, it is using Raleigh quotient which lead to the following equation:

$$\mathrm{filt}_{\mathrm{UMACE}} = D^{-1}m \qquad (29)$$

where D is the diagonal matrix same as that in conventional MACE filter. m is a column vector containing the mean values of the Fourier transform of the reference images.

The third type of MACE filter is the unconstrained optimal tradeoff synthetic discriminant filter (UOTSDF) shown by Refreiger [29] and Kumar et al [30] has yielding good verification performance. The UOTSDF is by:

$$\text{filt}_{\text{UOTSDF}} = (\alpha D + \sqrt{1-\alpha^2}C)^{-1}m \qquad (30)$$

where D is a diagonal matrix with average power spectrum of the training image placed along the diagonal elements. m is a column vector containing the mean values of the Fourier transform of the reference images. C is the power spectral density of the noise. White noise spectrum is the dominant source in predicting the performance of a thermal imaging system [31]. It is cause by the fluctuation in the detector output. Other noise sources (total up as background noise) are not that significant and normally limited /filter out by internal filter of some advanced thermal imaging system. For most of the applications, a white noise power spectral density is for assumption, therefore C reduces to the identity matrix. According to the derivation work done in [30], to determine the OTSDF, the authors minimize the energy function which obtains: $\alpha^2+\beta^2+\gamma^2+\delta^2=1$. In UOTSDF, the constant $\beta$, $\gamma$, $\delta \approx 0$. $\alpha$ term is typically set to be close to 1 to achieve good performance even in the presence of noise, however it also helps improve generalization to distortions outside the reference images.

The comparison work of the three correlation filters listed above is done in [5]. As a summary, UOTSDF is plan to extend into quaternion based thermal image correlator for the classification of
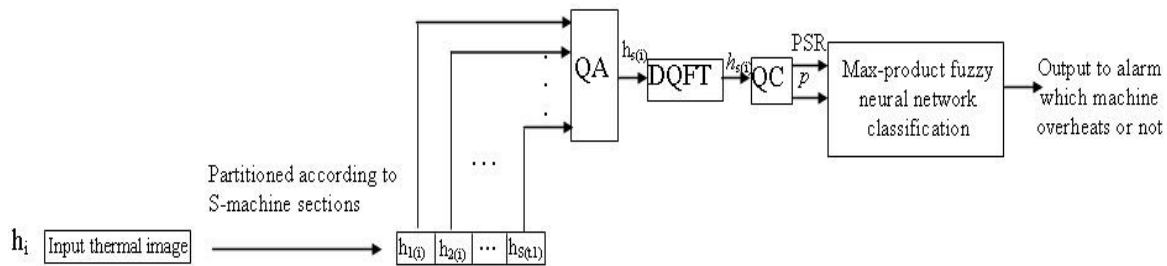


**FIGURE 10 :** Schematic of recognition stage

machine condition since it is less complicated in computational viewpoint than conventional MACE filter and achieve good performance.

### 4.3 Recognition Stage

The schematic of recognition stage for classification of machine condition by quaternion based thermal image correlator as proposed in [5] is shown in Fig. 10. To be applied in omnidirectional approach in this paper, during the recognition stage, live omnidirectional machines' image captured by omnidirectional thermal imaging system, unwarped into panoramic thermal image is first partitioned according to S machine sections. The partitioned image is then encoded into two dimensional quaternion array (QA) as follows [5]:

$$h_{s(i)} = h_{sr(i)} + h_{sR(i)}.i + h_{sG(i)}.j + h_{sB(i)}.k \qquad (31)$$

where i represents the input image, $h_{sr(i)}$ represents the real part of quaternion array of s-th machine section for input image i, s = 1, 2, …, S represents the number of partitioned machines' sections. $h_{sR(i)}$, $h_{sG(i)}$ and $h_{sB(i)}$ each represents the $i$-, $j$-, $k$- imaginary part of s-th machine section for input image i respectively.

The quaternion array in (31) is then performing DQFT to transforms the quaternion image to the quaternion frequency domain. A two-side form of DQFT is used [5]:

$$h_{s(i)}(m, n) = \sum_{\tau=0}^{M-1}\sum_{\eta=0}^{N-1} e^{-\mu_1 2\pi(m\tau/M)} . h_{s(i)}(\tau, \eta) . e^{-\mu_2 2\pi(n\eta/N)} \tag{32}$$

where $e$ is exponential term, $\mu_1$ and $\mu_2$ are two units pure quaternion as shown in (22) and (23) respectively. The output of the DQFT, $h_{s(i)}$ is cross correlated with every quaternion correlation filter in the database using the quaternion correlator (QC) just as the one shown in Fig. 8, but the DQFT output is now $h_{s(i)}$. In QC, performs quaternion correlation is performs on $h_{s(i)}$ with reference images $I_{s(t_2)}$ from database, and multiply with corresponding filter coefficients (filt$_{(t2)}$) [5]:

$$g_{s(i, t_2)}(m, n) = \sum_{\tau=0}^{M-1}\sum_{\eta=0}^{N-1} h_{s(i)} . \overline{I_{s(t_2)}(\tau - m, \eta - n)} . \text{filt}_{(t_2)} \tag{33}$$

After that, (33) is performing inverse DQFT to obtain the correlation plane function [5]:

$$P_{s(i, t_2)}(m, n) = \frac{1}{4\pi^2}\sum_{\tau=0}^{M-1}\sum_{\eta=0}^{N-1} e^{-\mu_1 2\pi(m\tau/M)} . g_{s(i, t_2)}(m, n) . \ e^{-\mu_2 2\pi(n\eta/N)} \tag{34}$$

Calculate $p_{s(i,t_2)}$ and $\text{PSR}_{s(i,t_2)}$ from the correlation plane as in (34) using (18) and (19) respectively. $p_{s(t_1,t_2)}$ means $p$-values of input image $h_{(i)}$ correlate on reference image $I_{(t_2)}$ in s-th machine section, while $\text{PSR}_{s(i,t_2)}$ means PSR values of input image $h_{(i)}$ correlate on reference image $I_{(t_2)}$ in s-th machine section. These values are then feed into max-product fuzzy neural network classifier to perform classification for machines' conditions, which will be presented in section 5.

## 5. MAX-PRODUCT FUZZY NEURAL NETWORK CLASSIFIER
Fuzzy logic is a problem solving system which is capable of dealing with approximate reasoning. Fuzzy logic provides high level of abstract through process which can appropriately handle the uncertainty in linguistic semantics, model expert heuristics and provide requisite high level organizing principles [32]. On the other hand, neural network is a computational biological network that can provides self organizing substrates for low level representation of information with adaptation capabilities. Both fuzzy logic and neural network are complimentary technologies and these two approaches is plausible to combine in the design of classification systems. Such integrated system is terms as fuzzy neural network classifier [32].

Many types of fuzzy neural network classifiers available in literature [33-36], and many fuzzy neural networks had been shown interest in applying max-min composition as functional basis [37-39]. However, Leotamonphong and Fang in their research work [40] mentioned that the max-min composition is "suitable only when a system allows no compensatability among the elements of a solution vector". They proposed to use max-product composition in fuzzy neural network rather than max-min composition. Research work done by Bourke and fisher in [41] also commented that the max-product composition gives better results than the traditional max-min operator. Subsequently, many efficient learning algorithms have been studied by others [42, 43] using the max-product composition.

Fuzzy neural network classifier using max-product composition for thermal image classification has been proposed in [5] for fixed angle machine condition monitoring system. In this paper, it will be once again repurposed for omnidirectional approached machine condition monitoring system.

### 5.1 Define 2 Classes, Namely: Overheat Class and Non-overheat Class
The reference images for all possible machines' conditions are captured, unwarped into panoramic form and stored in a database. Each of these reference images will be assigned with a unique number start from 1 till T, where T is the total number of reference images. These reference images are interpreted by an operator (human observer), the overall description of

which could be called the 'Operator perceived activity' (OPA)[44]. The operator will comments on each of the reference images and classified it into either overheat class or non-overheat class by storing the unique number of the reference images according to the classes respectively.

## 5.2 Training Max-product Fuzzy Neural Network Classifier

The max-product fuzzy neural network classifier is training with 4 steps [5]:

1.) $\mathrm{PSR}_{s(t_1,t_2)}$ and $p_{s(t_1,t_2)}$ output from the quaternion correlator of the enrollment stage are fuzzified through the activation functions (Gaussian membership function):

$$G_{\mathrm{PSR}_{s(t_1,t_2)}} = \exp\left[\frac{-\left(\mathrm{PSR}_{s(t_1,t_2)}-1\right)^2}{\sigma^2}\right] \qquad (35)$$

$$G_{p_{s(t_1,t_2)}} = \exp\left[\frac{-\left(p_{s(t_1,t_2)}-1\right)^2}{\sigma^2}\right] \qquad (36)$$

where $\sigma$ is the smoothing factor, that is the deviation of the Gaussian functions.

2.) Calculate the product value for s-th machine section of the fuzzy neural network classifier at each correlated images:

$$G_{s(t_1,t_2)} = G_{\mathrm{PSR}_{s(t_1,t_2)}} \times G_{p_{s(t_1,t_2)}} \qquad (37)$$

3.) Gather and store the product values in an array:

$$X_{s\,\mathrm{training}} = \begin{bmatrix} G_{s(1,1)} & G_{s(1,2)} & \cdots & G_{s(1,T)} \\ G_{s(2,1)} & G_{s(2,2)} & \cdots & G_{s(2,T)} \\ \vdots & \vdots & \ddots & \vdots \\ G_{s(T,1)} & G_{s(T,2)} & \cdots & G_{s(T,T)} \end{bmatrix} \qquad (38)$$

4.) The output will set so that it will output 1 if it is authentic class and 0 if it is imposter class, and it is in an array $Y_{\mathrm{identity}}$, whereby it is an identity matrix of dimension $T \times T$. To calculate the weight $w$ for s-th machine section, the equation is:

$$w_s = X_{s\,\mathrm{training}}^{-1} Y_{\mathrm{identity}} \qquad (39)$$

## 5.3 Max-product Fuzzy Neural Network Classification

The max-product fuzzy neural network classification is with 7 steps [5]:

1.) $\mathrm{PSR}_{s(i,t_2)}$ and $p_{s(i,t_2)}$ output from the quaternion correlator of the recognition stage are fuzzified through the activation functions (Gaussian membership function):

$$G_{\mathrm{PSR}_{s(i,t_2)}} = \exp\left[\frac{-\left(\mathrm{PSR}_{s(i,t_2)}-1\right)^2}{\sigma^2}\right] \qquad (40)$$

$$G_{p_{s(i,t_2)}} = \exp\left[\frac{-\left(p_{s(i,t_2)}-1\right)^2}{\sigma^2}\right] \qquad (41)$$

2.) Calculate the product value for s-th machine section of the fuzzy neural network classifier at input image on the training images in database:

$$G_{s(i,t_2)} = G_{\mathrm{PSR}_{s(i,t_2)}} \times G_{p_{s(i,t_2)}} \qquad (42)$$

3.) Gather and store the product values in an array:

$$X_{s\,classification} = \begin{bmatrix} G_{s(i,1)} & G_{s(i,2)} & \cdots & G_{s(i,T)} \end{bmatrix} \qquad (43)$$

4.) Obtain the classification outcomes for each machine condition in the s-th section by multiply (43) with the weight trained at (39):

$$Y_{s\,classification} = X_{s\,classification} \times w_s \qquad (44)$$

5.) Classify the input machine condition with the class of machine condition it belongs to by using max composition:

$$Class_s = \max\{Y_{s\,classification}\} \qquad (45)$$

6.) Determine which element in $Y_{s\,classification}$ matrix match with $Class_s$ :

$\psi$ = the position number of element in $Y_{s\,classification}$ matrix which has the equal value with $Class_s$ . $\qquad$ (46)

$\psi$ is corresponds to the assigned number of reference image in database.

7.) Based on two sets of fuzzy IF-THEN rules, perform defuzzification:

$R_s^1$: IF $\psi$ is match with the number stored in overheat class of s-th machine, THEN alarm: 'machine s overheat'. $\qquad$ (47)

$R_s^2$: IF $\psi$ is match with the number stored in non-overheat class of s-th machine, THEN alarm: 'machine s function properly'. $\qquad$ (48)

## 6. EXPERIMENTAL RESULTS
In this section, the application of log-polar mapper, quaternion based thermal image correlator together with max-product fuzzy neural network classifier is briefly illustrate for omnidirectional machine condition monitoring system. Here, some experiments are use to prove the algorithms introduced in section 3, 4 and 5.

### 6.1 Database of Reference Thermal Images for All Possible Machines' Condition.
A database with thermal images collected at the Applied Mecahnics Lab in Faculty of Engineering and Technology, Multimedia University is use to test the proposed quaternion based omnidirectional machine condition monitoring system. The database consists of panoramic thermal images unwrap from omnidirectional thermal images captured from three functioning machines by the use of omnidirectional thermal imaging system as shown in Fig. 2. A digital image captured with digital camera on the site is shown in Fig. 11, and a thermal image is also captured by the omnidirectional thermal camera set as shown in Fig. 12 at the same position based on all the functioning machines are in overheat condition. Comparing Fig. 11 and Fig. 12, observed that the material (mirror) good in IR reflection not necessary good in human visual range reflection. The corresponding panoramic form unwarped using log-polar mapping of Fig. 11 and Fig. 12 are shown in Fig. 13 and Fig. 14 respectively. In Fig. 13, machine A (leftmost one) and machine C (rightmost one) are vibro test machines with same model and same specifications, while machine B (center one) is a fatigue test machine. Three machines are considered to be overheating when their motors' temperature achieves 90°C.
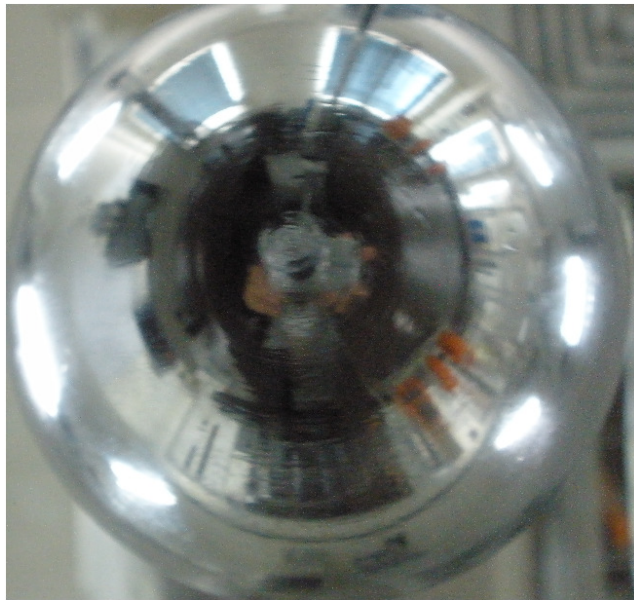
**FIGURE 11 :** Digital color form on site image
site image



**FIGURE 12 :** Thermal on



**FIGURE 13 :** Panoramic form of Fig. 11.



**FIGURE 14 :** Panoramic form of

The thermal images captured using FLIR ThermoVision A20M is with 320x240 display resolution pixels. Log-polar mapper will unwarp it into panoramic images with 282x60 display resolution pixels. The log-polar mapping process is by 4.54:1 reduction mapping scale, with almost four and a half fold data compression compare to original omnidirectional thermal image. Each machine section later partition into 94x60 pixels, as shown in Fig. 3. The database has T = 30 reference images, each with dimension 282 horizontal pixels × 60 vertical pixels of varying possible machines' conditions (temperature level with different color tones ranging from black, blue, purple, red, orange, yellow, light yellow to white) and can be divided into 8 major outcomes, namely: 1.) All machines function properly (none of the machines overheat), 2.) machine A overheat, 3.) machine B overheat, 4.) machine C overheat, 5.) machine A and machine B overheat, 6.) machine A and machine C overheat, 7.) machine B and machine C overheat, 8.) machine A, B, and C overheat.

### 6.2 Unconstrained Optimal Tradeoff Synthetic Discriminant Filter (UOTSDF) Used in Quaternion Based Thermal Image Correlator

The 30 reference images stored in database is use to synthesize a single UOTSDF using (30). D, m are calculated from the reference images and C is set as an identity matrix of dimension $30 \times 30$ and $\alpha$ set to 1. These values are substituted into (30) to calculate out the filter's coefficients. In enrollment stage, for each filter line as in Fig. 8, cross correlations are performed on all the DQFT form of reference images in database ($I_{s(t_1)}$) with the DQFT form of reference images in database as well ($I_{s(t_2)}$), and multiply the output value with corresponding filter coefficients respectively, where $t_1$, $t_2$ = 1, 2, ..., 30; s = 1, 2, 3. In recognition stage, for each filter line, cross correlation are also performed on the DQFT form of input image ($h_{s(i)}$) with the DQFT form of reference images in database ($I_{s(t_2)}$) and multiply the output value with corresponding filter coefficients respectively. For authentic case (good match in between two images), the correlation plane should have sharp peaks and it should not exhibit such strong peaks for

imposter case (bad or no match in between two images). These two cases will be investigated below:

Authentic case: Fig. 16a-16c show the samples correlation plane for input thermal image (for every machine is overheat, as in Fig. 15) matching with one of the reference image of overheat class in the database, for section machine A, section machine B and section machine C respectively. Since the three pairs of images are in good match, their correlation planes are having smooth and sharp peaks.
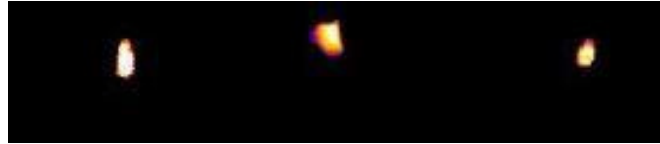


**FIGURE 15 :** Sample input thermal image (all machines overheat)
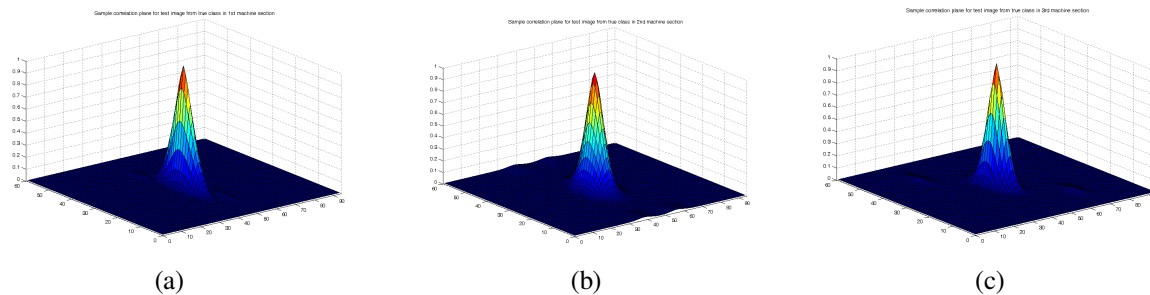


|  (a)  |  (b)  |  (c)  |

**FIGURE 16 :** Samples correlation plane for input thermal image (for every machine is overheat) matching with one of the reference image of overheat class for both all the machines in the database (authentic case) a.) section machine A, b.) section machine B, c.) section machine C.

Imposter case: Fig. 18a-18c show the samples correlation plane for input thermal image (for every machine is not –overheat as in Fig. 17) matching with one of the reference image of overheat class in the database (as in Fig. 12), for section machine A, section machine B and section machine C respectively. Since the three pairs of images are not in good match, their correlation planes are having no sharp peak at all.
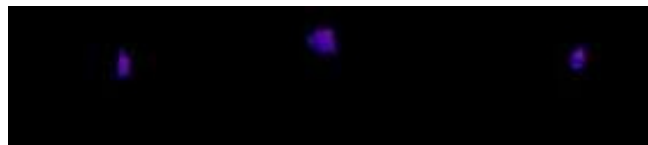


**FIGURE 17 :** Sample input thermal image (all machines not overheat)
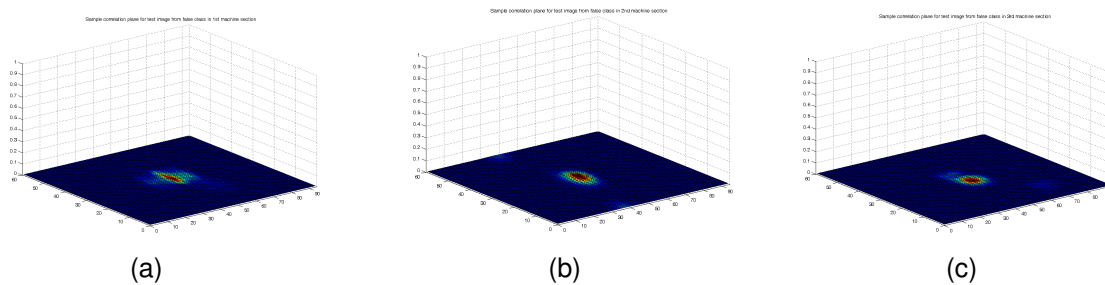


|  (a)  |  (b)  |  (c)  |

**FIGURE 18 :** Samples correlation plane for input thermal image (for every machine is not-overheat) matching with one of the reference image of overheat class for both all the machines in the database (imposter case) a.) section machine A, b.) section machine B, c.) section machine C.

Table 1 shows the PSR and p-value for both authentic and imposter case as in Fig. 16 and Fig 18 for section machine A, B and C. Note that the sharp correlation peak resulting in large normalized PSR and *p*-value in authentic case of section machine A, B and C, whereas small PSR and *p*-value exhibiting in the imposter case of section machine A, B and C.

**TABLE 1:** Normalized PSR and p-values for both authentic and imposter case.

| Authentic case | Normalized PSR | Normalized p-value | Imposter case | Normalized PSR | Normalized p-value |
|---|---|---|---|---|---|
| Section mac. A | 0.9820 | 0.9886 | Section mac. A | 0.0453 | 0.0363 |
| Section mac. B | 0.9437 | 0.9836 | Section mac. B | 0.0365 | 0.0315 |
| Section mac. C | 1.0000 | 0.9947 | Section mac. C | 0.0489 | 0.0375 |

### 6.3 Efficiency of the Quaternion Based Machine Condition Monitoring System

The quaternion based omnidirectional machine monitoring system was evaluated with respect to the thermal images captured live, unwarped into panoramic form and displayed on monitor screen as interpreted by a operator (human observer) the overall description of which could be called the 'operator perceived activity' (OPA) [45]. The operator will comments on the unwarped panoramic images captured by the omnidirectional thermal imaging system, whether any of the machines are overheat or not and compare with that classified by the proposed machine condition monitoring system. The system was evaluated for 10,000 samples images captured by the omnidirectional thermal imaging system for monitoring the functioning machines as in Fig. 11. Among the total 10,000 samples images, 9,702 were tracked perfectly (output machines' conditions agreed by both observer and the machine condition monitoring system), i.e. an overall accuracy of 97.02%.

## 7. CONCLUSIONS

This paper presented an omnidirectional machine condition monitoring system capable of monitoring machine condition in a wide area coverage using minimum hardware manner, whereby the machines surrounded in an omnidirectional (360°) view can be monitored by using a single thermal camera and a custom made hyperbolic IR mirror. The proposed machine condition monitoring system also using log-polar mapper unwarping 320x240 omnidirectional thermal images into 282x60 panoramic image, providing observer or image processing tools a wide angle of view and with data compression upto 4.5 folds. Therefore, log-polar mapping helps reduces the computation time in image processing and memory storage needs. Quaternion thermal image correlation method deals with color thermal images without converting them into gray-scale images. This can better preserved important color information. Max-product fuzzy neural network is a high level framework for approximate reasoning, best suit to be used in classification of machine conditioning. Experimental results show that the proposed machine condition monitoring system is with accuracy as high as 97 %. The experimental results show that the apply of PSR and *p*-value give higher accuracy in tracking thermal condition for the proposed quaternion based omnidirectional machine condition monitoring system. In future, collaboration is plan seek for implementing the proposed quaternion based omnidirectional machine condition monitoring system in fossil power plant monitoring. The omnidirectional scenes in a site of turbine room, steam pipework system, boilers, high pressure by-pass drain valve etc within a fossil power plant can be monitored effectively with such system. A trespasser detection algorithm is also plan to develop for trespasser detection purpose. All these topics will be addressed in future work.

## REFERENCES

[1]    W. K. Wong, P. N. Tan, C. K. Loo and W.S. Lim, "An Effective Surveillance System  Using Thermal Camera",  2009 International Conference on Signal Acquisition and Processing (ICSAP 2009), 3-5, Apr 2009, Kuala Lumpur, Malaysia: 13-17.

[2]    F. Berton, A brief introduction to log-polar mapping, Technical report, LIRA-Lab, University of Genova, (Feb 2006).

[3]    C. Xie, M. Savvides and B.V.K. Vijaya Kumar, "Quaternion correlation filters for face recognition in wavelet domain", Int. Conf. on Accoustic, Speech and Signal Processing (ICASSP 2005):II85- II88.

[4]    S. C. Pei, J. J. Ding and J. Chang, "Color pattern recognition by quaternion correlation", Proc. of Int. Conf. on Image Processing, Vol.1, (2001) : 894-897.

[5]    W. K. Wong, C. K. Loo, W. S. Lim, P. N. Tan, "Thermal Condition Monitoring System Using Log-Polar Mapping, Quaternion Correlation and Max-Product Fuzzy Neural Network Classification", Elsevier, Neurocomputing (in press).

[6]    B.V.K. Vijaya Kumar, M. Savvides, K. Venkataramani and C. Xie, "Spatial frequency domain image processing for biometric recognition", Proc. Of Int. Conf. on Image Processing, Vol.1, (2002) p.p. I53-I56.

[7]    R.O. Duda, P.E. Hart and D.G. Stork, Pattern Classification, 2nd Ed. Wiley, N.Y, 2001.

[8]    R.K. Brouwer, "A fuzzy threshold max-product unit, with learning algorithm, for classification of pattern vectors", Proc. of the VI Brazillian Symp. On Neural Networks, (Jan 2000) p.p. 208-212.

[9]    S. Gatcher, "Mirror Design for an Omnidirectional Camera with a Uniform Cylindrical Projection When Using the SVAVISCA Sensor", Research Reports of CMP, OMNIVIEWS Project, Czech technical University in Prague, No. 3, 2001. Redirected from: http://cmp.felk.cvut.cz/projects/omniviews/

[10]    http://www.flirthemography.com

[11]    H. Araujo, J. M. Dias, "An Introduction To The Log-polar Mapping", Proceedings of 2nd Workshop on Cybernetic Vision, 1996, p.p. 139-144.

[12]    C. F. R. Weiman and G. Chaikin, "Logarithmic Spiral Grids For Image Processing And Display", Computer Graphics and Image Processing, Vol. 11, 1979, p.p. 197-226.

[13]    W. K. Wong, P. N. Tan, C. K. Loo and W. S. Lim , "Machine Condition Monitoring Using Omnidirectional Thermal Imaging System", IEEE International Conference on Signal & Image Processing Applications 18-19, November 2009, Kuala Lumpur, Malaysia, Paper No. 151, p.p. 1-6.

[14]    R. Wodnicki, G.W. Roberts, and M.D. Levine, "A foveated image sensor in standard CMOS technology", Custom Integrated Circuits Conf. Santa Clara, May 1995, p.p. 357-360.

[15]    F. Jurie, "A new log-polar mapping for space variant imaging: Application to face detection and tracking", Pattern Recognition,Elsevier Science, 32:55, 1999, p.p. 865-875.

[16]    M. Bolduc and M.D. Levine, "A review of biologically-motivated space variant data reduction models for robotic vision", Computer Vision and Image Understanding, Vol. 69, No. 2, (February 1998) p.p. 170-184.

[17]    C.G. Ho, R.C.D. Young and C.R. Chatwin, "Sensor geometry and sampling methods for space variant image processing", Pattern Analysis and Application, Springer Verlag, (2002) p.p. 369-384.

[18]    W. R. Hamilton, Elements of Quaternions, London, U.K.: Longmans, Green (1866).

[19]   T.A. Ell, "Quaternion-Fourier transforms for analysis of two-dimensional linear time-invariant partial differential systems", Proc. of 32nd Conf. Decision Contr., (Dec 1993) p.p. 1830-1841.

[20]   T.A. Ell, "Hypercomplex spectral transforms", PhD dissertation, Univ. Minnesota, Minneapolis, 1992.

[21]   S.C. Pei, J.J. Ding and J.H. Chang, "Efficient implementation of quaternion Fourier transform convolution and correlation by 2-D Complex FFT", IEEE Trans. on Signal Processing, Vol. 49, No. 11, (Nov 2001) p.p. 2783-2797.

[22]   S.J. Sangwine and T.A. Ell, "Hypercomplex auto- and cross-correlation of colour images", Proc. of Int. Conf. on Image Processing, (ICIP 1999) p.p. 319-323.

[23]   T.A. Ell and S.J. Sangwine, "Colour –sensitive edge detection using hypercomplex filters", (EUSIPCO 2000) p.p. 151-154.

[24]   A Vanderlugt, "Signal detection by complex spatial filtering", IEEE Trans. Inf. Theory, Vol. 10, (1964) p.p.139-145.

[25]   M. Saviddes, K. Venkataramani and B.V.K. Vijaya Kumar, "Incremental updating of advanced correlation filters for biometric authentication systems", Proc. of Int. Conf. on Multimedia and Expo, Vol. 3 (ICME 2003) p.p. 229-232.

[26]   A. Mahalanobis, B.V.K. Vijaya Kumar and D. Casasent, "Minimum average correlation energy filters", Applied Optics, Vol. 26, (1987) p.p. 3633-3640.

[27]   M. Savvides, B.V.K. Vijaya Kumar and P. Khosla, "Face verification using correlations filters", Procs of 3rd IEEE Automatic Identification Advanced Technologies, Tarrytown, N.Y., (2002) p.p. 56-61.

[28]   A. Mahalanobis, B.V.K. Vijaya Kumar, S.R.F. Sims and J.F. Epperson, "Unconstrained correlation filters", Applied Optics, Vol. 33, (1994) p.p. 3751-3759.

[29]   P. Refreiger, "Filter design for optical pattern recognition: multi-criteria optimization approach", Optics Letters, Vol. 15, (1990) p.p. 854-856.

[30]   B.V.K. Kumar, D.W. Carlson, and A. Mahalanobis, "Optimal trade-off synthetic discriminant function filters for arbitrary devices", Optics Letters, Vol. 19, No. 19, (1994) p.p. 1556-1558.

[31]   H. V. Kennedy, "Modeling noise in thermal imaging systems", Proc. of SPIE, Vol. 1969, (1993), p.p. 66-70.

[32]   S. Kumar, Neural Networks: A Classroom Approach, McGraw Hill, Int. Ed., 2004.

[33]   J.J. Buckley and Y. Hayashi, "Fuzzy neural networks: A survey", Fuzzy Sets and Systems, 66, (1994) p.p. 1-13.

[34]   C.T. Lin and C.S.G. Lee, Neural Fuzzy Systems: A Neuro-Fuzzy Synergism to Intelligent Systems, Prentice Hall, Upper Saddle River, N.J., 1996.

[35]   D. Nauck, F. Klawonn and R. Kurse, Foundations of Neuro-Fuzzy Systems, Wiley, Chichester, U.K., 1997.

[36]   S.K. Pal and S. Mitra, Neuro-Fuzzy Pattern Recognition: Methods in Soft Computing, Wiley, Chichester, U.K., 1999.

[37]   R. Ostermark, "A Fuzzy Neural Network Algorithm for Multigroup Classification", Elsevier Science, Fuzzy Sets and Systems, 105, (1999) p.p. 113-122.

[38]  H.K. Kwan and Y. Cai, "A Fuzzy Neural Network and its Application to Pattern Recognition", IEEE Trans. on Fuzzy Systems, 2(3), (1997) p.p. 185-193.

[39]  G.Z. Li and S.C. Fang, "Solving interval-valued fuzzy relation equations", IEEE Trans. on Fuzzy Systems, Vol. 6, No. 2, (May 1998) p.p. 321-324.

[40]  J. Leotamonphong and S. Fang, "An efficient solution procedure for fuzzy relation equations with max product composition", IEEE Trans. on Fuzzy Systems, Vol. 7, No. 4, (Aug 1999) p.p. 441-445.

[41]  M.M. Bourke and D.G. Fisher, "A predictive fuzzy relational controller", Proc. of the Fifth Int. Conf. on Fuzzy Systems, (1996) p.p. 1464-1470.

[42]  M.M. Bourke and D.G. Fisher, "Solution algorithms for fuzzy relational equations with max-product composition", Fuzzy Sets Systems, Vol. 94, (1998) p.p. 61-69.

[43]  P. Xiao and Y. Yu, "Efficient learning algorithm for fuzzy max-product associative memory networks", SPIE, Vol. 3077, (1997), p.p. 388-395.

[44]  J. Owens, A. Hunter and E. Fletcher, "A Fast Model–Free Morphology–Based Object Tracking Algorithm", British Machine Vision Conference, p.p. 767-776, 2002.